Thin Solid Films 654 (2018) 54–60

Contents lists available at ScienceDirect

Thin Solid Films

journal homepage: www.elsevier.com/locate/tsf

Morphology and optical properties of Ge nanocrystalline films grown by nonequilibrium epitaxy on Si (001) surface

V.S. Lysenko[a], S.V. Kondratenko[b], Yu.N. Kozyrev[c], V.P. Kladko[a], O. Yo. Gudymenko[a], V.V. Strelchuk[a], A.S. Nikolenko[a], O.S. Kondratenko[a], S.A. Iliash[b,*], G.S. Pekar[a]

[a] Institute of Semiconductor Physics, 41 Prospect Nauki, 03028 Kyiv, Ukraine
[b] Taras Shevchenko National University of Kyiv, 64 Volodymyrs'ka St., 01601 Kyiv, Ukraine
[c] O.O. Chuiko Institute of Surface Chemistry, 17 Generala Naumova St., 03164 Kyiv, Ukraine

ARTICLE INFO

Keywords:
Thin films
Morphology
Ge nanocrystalline films
Raman spectroscopy
Optical properties
X-ray diffraction

ABSTRACT

Optical properties and morphology of thin films with Ge and SiGe nanocrystallites are studied by using the methods of Raman scattering, multi-angle ellipsometry, and X-ray measurements. Our observations showed that low-temperature Ge epitaxy on Si(001) surface at 350 °C and at high growth rate leads to the formation of thin films consisting of Ge nanocrystallites with the porosity of about 50%. Deposition of Si adatoms on the film surface stimulates the reconstruction of the surface with nanocrystallites and results in the increase of the degree of Ge crystallinity, coalescence of adjacent nanocrystallites, and in a slight Si-Ge mixing. The change in the values of the optical constants due to silicon deposition is described by means of Bruggeman approximation. The main reasons for these changes are the film crystallization and the appearance of Si crystalline phase in the structures with Si capping layer. The prepared Ge nanocrystalline solids, as well as the films covered with Si, may be used in quantum dot solar cells due to the high absorption capacity of the films and devices working in the hopping regime.

1. Introduction

Thin films with Ge nanocrystallites (NCs) attract an interest due to new possibilities for many electronic applications, including field-effect transistors [1], IR photodetectors, and solar cells [2–9]. The main reason is strong quantum confinement in the Ge NCs leading to size dependent optical properties as well as larger absorption coefficient and higher luminescence efficiency compared with bulk Ge [10]. Meanwhile, the Ge NC thin films have particular advantages due to high electron and hole mobilities ($\mu_e = 3900\,cm^2\,V^{-1}\,s^{-1}$, $\mu_h = 1900\,cm^2\,V^{-1}\,s^{-1}$) and increased electrical conductivity when charge transport is affected by the hopping processes [11]. All these circumstances stimulate special interest in development of new synthesis approaches for high-density array of Ge NCs, focusing on decrease the distance between the NCs and narrowing the dispersion of NC sizes. Moreover, the morphology and optoelectronic properties of such films can be easily varied within a wide range by deposition of Si adatoms on surface with Ge NCs.

Of particular interest are nanocrystalline SiGe and Ge films grown on silicon substrates, due to their compatibility with silicon technology. Electronic spectrum, charge carrier transport and optical properties of SiGe-based nanostructures depend essentially on the strain, owing to mismatch of parameters of Si and Ge crystal lattices as well as to variations in the size and composition of Ge nanostructures. This opens possibilities for creating nanocrystalline thin films with predetermined properties for applications in optoelectronics, photovoltaics and sensors [12,13].

Heterostructures with SiGe NCs on Si(001) surface are usually obtained by the method of molecular beam epitaxy in the Stranski-Krastanov mode, which differs by a sharp transition from two-dimensional (2D) growth to the 3D growth of NCs [2,14,15]. In this case, a key factor is the energy gain due to reducing the mechanical stress resulted from the changes in film topology. At the initial stage of semiconductor material deposition on the surface of the crystal with a smaller lattice constant, the layered growth can occur. The first few layers grow pseudomorphically, according to the van der Merwe mechanism [16], which involves the formation of the so-called wetting layer [17]. As a result of the difference in the lattice constants, the growing Ge film is compressed in the plane of the substrate, which modifies essentially their optical and electronic properties [18–20].

The elastic energy of the film increases with its thickness, and when exceeding a certain critical thickness, which is called the thickness of

* Corresponding author.
E-mail address: iliashsviatoslav@gmail.com (S.A. Iliash).

https://doi.org/10.1016/j.tsf.2018.03.089
Received 30 May 2017; Received in revised form 22 March 2018; Accepted 30 March 2018
Available online 03 April 2018
0040-6090/

the wetting layer, a relaxation of elastic stresses occurs due to an appearance of three-dimensional islands [2]. The formation of pre-pyramids, followed by pyramids, domes, barns [21] and finally cupolas [22] has taken place depending on the amount of deposited Ge and growth conditions. This allows growing an array of Ge NCs with a surface density up to 10^{11} cm^{-2} [2], which is insufficient for successful practical application of nanocrystalline film due to low density of states. Deposition of one monolayer of Sb or C atoms [23] as well as oxidation of Si(001) surface allowing to achieve a NC density as high as 10^{12} cm^{-2}–10^{13} cm^{-2} [24].

The idea of the performed experiment was to modify Stranski-Krastanov (S-K) growth mode in order to create thin films with a thickness of tens or hundreds nanometer, which contains dence array of the Ge NCs with a diameter ~10 nm or less and distances between neighboring NCs required for a strong quantum confinement and tunable coupling. The optical properties and morphology of thin films with Ge NCs as well as their changes due to Si adatoms deposition on their surface have been studied. It is found that the size and the shape of Ge NCs depend on the growth temperature, indicating the significant influence of the surface processes kinetics on the morphology of Ge films. The process of spontaneous formation of Ge NCs, particularly S-K mode, is described in detail for the case of thermodynamic equilibrium when the film morphology is independent of the kinetic parameters of the surface. However, at lower temperatures and the significant increase in the Ge deposition rate, another growth mode is also possible. At the initial stage, the transition from the two-dimensional to three-dimensional growth occurs, which leads to the formation of NCs arrays with high (about 10^{11} cm^{-2}) surface density. The combination of low growth temperature (about 350 °C) which limits the surface migration of Ge adatoms, with the high growth rate (about 5 nm/min) creates conditions for the formation of Ge NCs on the surface of previously formed NCs. As a result, we have managed to prepare nanostructured solids with the high density of Ge NCs with a diameter of 5–6 nm. Such solids are extremely important for the design of devices working in the hopping regime [25] as well as devices with improved characteristics due to quantum confinement and tunneling effect.

2. Experimental details

The molecular beam epitaxy (MBE) technique was used to prepare monolayer and multilayer Ge–Si(100) NC arrays with the clusters of various sizes and surface density. The (100) oriented wafers of p-Si with resistivity of 7.5 Ω·cm and diameter of 76 mm were used as substrates. The accuracy of the orientation was better than 1°. The growth process was controlled via RHEED (reflection high energy electron diffraction) by recording the intensity oscillations of the central reflected beam.

Evaporators heated by electron bombardment generated the Si and Ge beams. The evaporators were constructed as autocrucibles and operated in the mode where the evaporation rate was proportional to the electron-beam power. The chemical composition of the molecular beams was checked with a quadrupole mass-spectrometer. The background pressure of residual gases in the MBE set-up was $6{\cdot}10^{-10}$ Torr, which was increased by about $3{\cdot}10^{-10}$ Torr as Si or Ge evaporators were switched on. After desorption of the passivating Si oxide film from the Si substrate, which was exposed to a Si beam of a weak intensity and kept at 800 °C during this process, a buffer Si film, about 0.1–0.5 μm thick, was deposited onto the Si surface. This film produced a high-contrast Si(100) 2 × 1 RHEED pattern typical of clean Si.

The Ge nanocrystalline layers were deposited at 350 °C (structure A). After deposition of Ge NCs, half of the wafer was covered by a mask, and the system was exposed to a weak flow of Si ions. As a result, SiGe NCs were formed on the uncovered part of the wafer due to additional deposition of silicon with a nominal thickness of about 5 monolayers (MLs) (structure B). Finally, a part of the wafer with as-grown Ge NCs was covered by 65 nm thick Si layer (structure C). The growth rate was 0.15 nm/min for Si and 5.0 nm/min for Ge. As a results, three different structures were grown on common Si(100) wafer.

Different experimental techniques were employed to characterize the size of NCs. Size distribution and surface densities of the NCs as well as the RMS values of their surfaces were controlled using atomic force microscopy (AFM) by scanning uncovered structures grown at the same conditions. AFM measurements were performed with an NT-MDT Ntegra microscope in semi-contact tapping mode using Si cantilevers with a tip apex radius of about 10 nm.

X-ray diffraction (XRD) measurements were performed by using PANalyticalX'Pert Pro MRD diffractometer (PANalytical, Almelo, the Netherlands) equipped with an X-ray tube with Cu Kα1-radiation (λ = 1.540598 Å), symmetric 4 × Ge(220) monochromator and a channel-cut Ge(220) analyzer. To study these structures, the high-resolution X-ray diffraction (HRXRD) was used, and the reciprocal space maps of symmetric (004) and asymmetric (113) reflexes were obtained. The curves of diffraction reflection parallel and perpendicular to reciprocal lattice vector (2θ-ω and ω-scanning) were recorded in three-crystalline mode. In addition, by the mean of the X-ray reflectometry, the curves of the of X-rays mirror reflection from the sample surface were recorded.

Multiple-angle-of incidence (MAI) ellipsometric measurements were done using LEF-3M null-ellipsometer with a fixed compensator and He-Ne laser as a light source (λ = 632.8 nm) with a spot size about 1 mm × 2 mm. By fitting the experimental curves of ellipsometric angles Ψ(ϕ) and Δ(ϕ) to theoretical ones using a one-layer structural model "ambient–film–substrate", the effective optical constants $n = n + ik$, permittivities $\varepsilon = \varepsilon_1 + i\varepsilon_2$, and the thicknesses of SiGe layers have been calculated under the assumption of their isotropy and homogeneity.

Micro-Raman spectra were recorded at room temperature using a computer-controlled Raman spectrometer T-64000 Horiba Jobin-Yvon equipped with a thermoelectrically cooled CCD detector. Excitation was performed with 488 nm line of Ar-Kr ion laser with a power on the sample surface of about 1 mW. Micro-Raman spectra were measured in the backscattering from (100) plane in the crossed $z(x,y)\bar{z}$–geometry, where x, y and z correspond to {100}, {010} and {001} directions of the cubic crystal structure, correspondingly. The radiation was focused by an Olympus long focus objective, 50X, NA = 0.5. Such a geometry was chosen because it allows for scattering on LO phonons in germanium and silicon whereas two-phonon scattering on TA phonons in the Si substrate is forbidden.

3. Results and discussion

Fig. 1 shows the AFM images of the surface of the structure A consisting of the nanocrystalline Ge film on Si (001) surface. The average diameter of NCs was 28 nm and their surface density was $1.1{\cdot}10^{11}$ cm^{-2}. After 5 ML Si deposition on the surface of the structure A, the reconstruction of the surface with nanocrystals occurred followed by the coalescence of the adjacent NCs as well as by the increase of the average nanocrystal size up to 35 nm and by the decrease of the surface density of NCs to $0.7{\cdot}10^{11}$ cm^{-2}. AFM images of such surface of the B structure are shown in Fig. 1b. The resulting histograms of the distributions of NC diameters was approximated by a Gaussian distribution with a width FWHW equal to 28 nm and 38 nm for A and B structures, respectively (see Fig.1c, d). Comparing the size distributions obtained, one can conclude that after Si deposition on the surface with Ge NCs, the smaller NCs disappear predominantly. This may be due to the coalescence of the adjacent Ge NCs stimulated by Si adatoms. Obviously, this process will be the more efficient the smaller the size of the NCs.

In addition to increasing of FWHW after deposition of Si on the surface of the Ge films, the change of the shape of the NCs' bases was observed. The base of the formed NCs is no longer circular after surface reconstruction, but becomes polygonal with sides oriented along [100] and [010] directions.

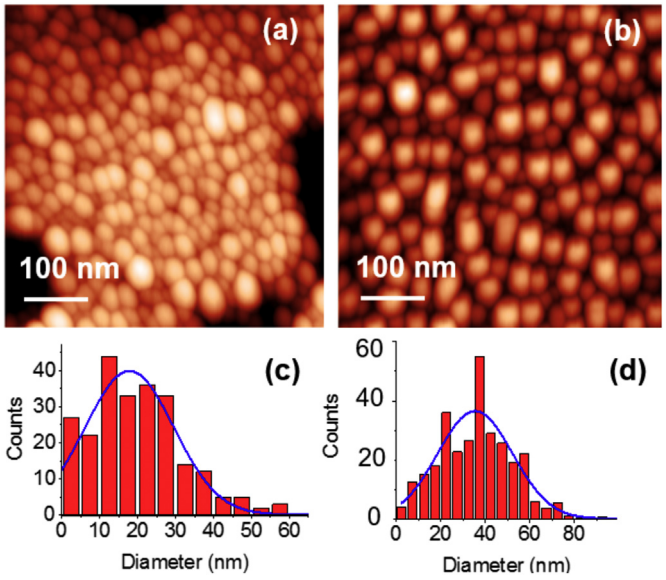

Fig. 1. AFM images of (a) the nanocrystalline Ge films on Si (001) (structure A) and (b) after coating the surface with 5 ML of Si (structure B). Diameter distributions of the NCs of Ge films on Si(001) before (c) and after (d) deposition of 5 ML of Si.

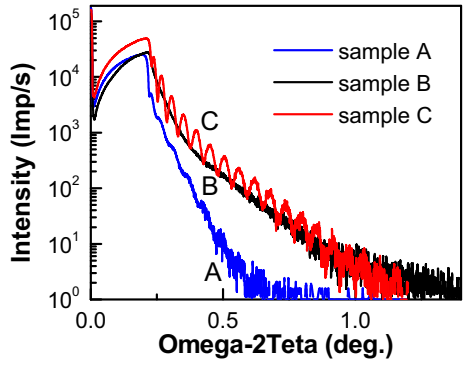

Fig. 2. (a) X-ray reflectivity profile for the structures with Ge nanocrystallites grown on Si (001) wafer (structure A); (b) the same after additional deposition of Si with a nominal thickness of about 5 MLs on structure with Ge nanocrystallites (structure B); and X-ray reflectivity profile for structure C with Ge nanocrystallites covered by 65 nm thick Si layer.

Fig. 2 shows the X-ray reflectivity profile for the Ge nanocrystalline films grown on the Si(001) substrate. Fitting of measured profiles gives information about thicknesses, mass density and interface roughness of the Ge thin films. From the period of the oscillations at the mirror curve of the X-ray reflectometry of the structure A, the thickness of the Ge film was determined. It turned out to be 59 nm and the critical angle $\theta_c = 0.216°$.

The obtained value of θ_c allowed determining the value of mass density using Snell's law:

$$\theta_c = \sqrt{\frac{\lambda^2}{\pi}\frac{Z\rho N_A}{M}}, \quad (1)$$

where M is the molar mass, N_A is the Avogadro constant, λ is the wavelength, ρ is the mass density.

It was established that the film density of the structure A equals to 2.56 g/cm^3, which may be due to the porosity of the film whose surface topology is shown in Fig. 1. Its density is smaller than that of the bulk Ge crystal (ρ_{bulk} = 5.35 g/cm^3). The porosity P can be deduced from the mass-density ρ of the Ge thin films, using the following equation:

$$\rho = \rho_{bulk}(1 - P). \quad (2)$$

Hence, the overall porosity of the structure A was found to be about 50%.

Reduction of the amplitude of the intensity oscillations in Fig. 2 (curve A compared with curve C) could be considered as evidence of the sharp increase in surface roughness of the film with nanocrystallites. An abrupt decrease of the intensity in the region of angles exceeding the critical one (above 0.3) is evidence of a sharp increase of the surface roughness. A rapid damping of oscillations of the X-ray reflectivity profile and a strong drop in intensity at high angles of incidence allows to estimate the roughness (RMS) of the studied Ge film (structure A) to be about 1.8 nm for the Si(001)-substrate/Ge film interface, and about 2.6 nm for the Ge film/air interface.

The surface roughness determined from the analysis of AFM image for the structure A gives the RMS values of 3.6 nm for the Ge–air interface. The value of roughness measured by AFM can be larger than that determined from the X-ray reflectivity [26] due to the presence of the oxide coverage of the Ge NCs and of the amorphous phase, which does not contribute to the X-ray signal. Thereby, the RMS values for Ge-air and Ge-Si interfaces give reason to assume that the investigated films consist of the nanocrystallites. Regarding the structure B, it can be concluded that its surface roughness is comparable with that of the structure C, and the absence of oscillations (their weak visibility) can be associated with a surface roughness of SiGe NCs.

By approximating the X-ray reflectometry curves for the structure C on the base of the Raman scattering data, the presence of the $Si_{0.5}Ge_{0.5}$ interfacial layer between the Ge nanocrystalline film and Si capping layer was considered, which allowed us to obtain a good agreement between the experimental and theoretical curves of mirror reflection. As a result of this procedure, the following parameters of the structure were obtained: the intermediate $Si_{0.5}Ge_{0.5}$ layer has a thickness of 6.5 nm, a density of 3.076 g/cm^3, a roughness of about 4.5 nm and strain value of $\varepsilon_{xx} = -0.009$. Taking into account those parameters, the density of the bulk $Si_{0.5}Ge_{0.5}$ alloy was obtained to be about 3.23 g/cm^3, the porosity of this layer was P = 5% (or filling factor f = 95%).

This means that at Si deposition, the cavities in Ge films are filled by Si adatoms which is accompanied by the significant silicon-germanium mixing and by the formation of a $Si_{0.5}Ge_{0.5}$ solid solution. The observed porosity ~5% may be due to the fact that some part of the cavities in the film remains unfilled or is non-crystalline, and therefore does not contribute to the measured X-ray signal.

Fitting of the X-ray reflectivity profile gave the thickness of the Si capping layer of 65.9 nm, while roughness of the Si/air interface was about 1.02 nm. In addition, the upper silicon layer was completely relaxed and compressive strain in the intermediate $Si_{0.5}Ge_{0.5}$ layer was Δa ~ $-6{,}2\cdot10^{-3}$ Å or $\varepsilon_{xx} = -0.011$. Note that the strain value was estimated based on the lattice constant of the bulk $Si_{0.5}Ge_{0.5}$ alloy, which equals to 5.494 Å, according to Vegard's rule.

Fig. 3 shows the reciprocal space maps (RSMs) near the Si(113) Bragg peak for all structures - A, B and C. Since the RSM oscillations in asymmetric (113) reflexes oriented along the normal to the surface, and are located along one line (along the coordinate axes which determines the lateral lattice parameter) with a reciprocal lattice site which belong to the silicon substrate (e.g. Fig. 4), it can be concluded, that the layers are pseudomorphic to Si(001) [27,28]. It is worth noting that the oscillation maximums are not due to diffraction on Ge thin layers, but are due to phase modulation caused by them. Compared to the initial sample, the oscillation patterns for the structure B proved to be more clear which is evidence of Ge film crystallization at Si deposition.

After formation of the capping layer of the structure C, RSM near the 113 peak is peculiar to a more structured surface. It can be seen that the main peak becomes narrower in the lateral direction with the appearance of symmetrical tails in the lower part, which is a structuring feature. The manifestation of oscillations seems somewhat less clear due to the increased thickness of the structure (reduction of the period of

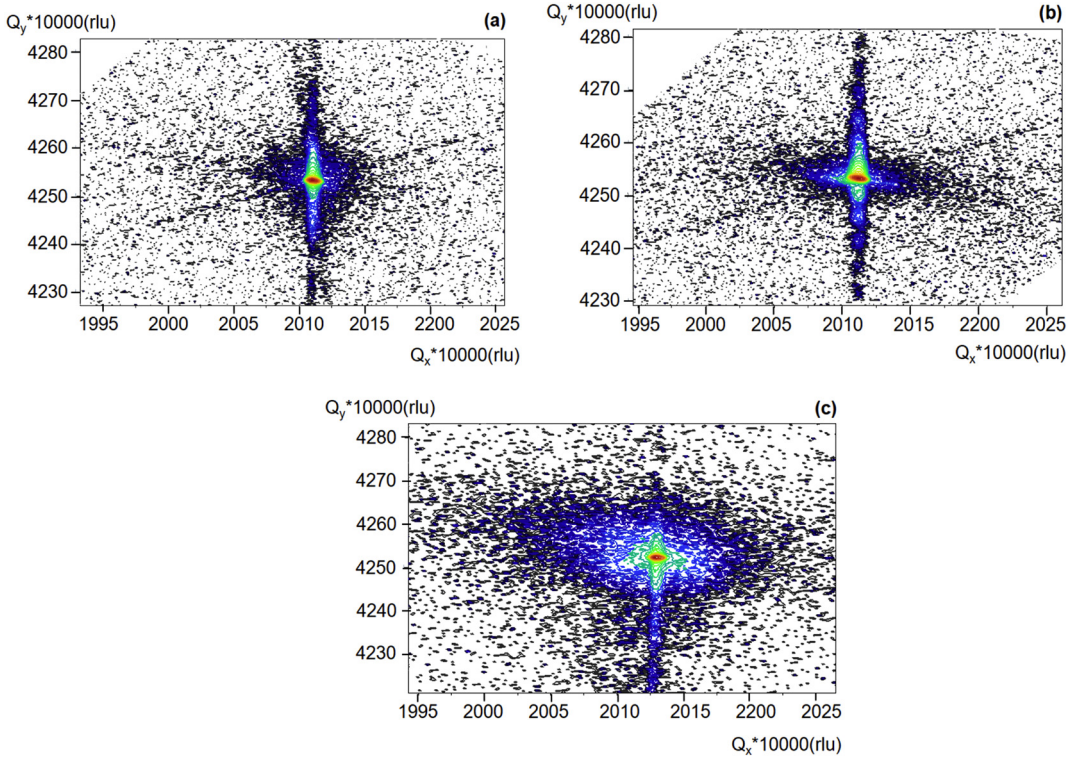

Fig. 3. Asymmetric RSMs from (113) reflection: (a) structure A, (b) structure B, (c) structure C.

oscillation).

The experimental angle dependencies of the ellipsometric angles Ψ(ϕ) and Δ(ϕ) are presented in Fig. 4. For calculation of the optical constants of structure A, we used two-component layer on the Si substrate surface: Ge and voids, while three-component model (Ge, Si, and voids) was used for structure B. By solution of the inverse spectroscopic problem, the effective optical constants $\tilde{n} = n + ik$ of surface layer with Ge NCs and its thickness, d_{eff}, were determined (Table 1). The following constants were obtained: $n = 3.91$, $k = 0.61$, $d_{eff} = 67.8$ nm for the structure A and $n = 3.94$, $k = 0.72$, $d_{eff} = 80.0$ nm for the structure B. The optical constants at $\lambda = 632.8$ nm are $n = 5.29$, $k = 0.64$ for bulk Ge and $n = 3.885$, $k = 0.012$ for bulk Si [29]. Somewhat smaller values of effective optical constants of the studied films as compared with the tabulated Ge values are due to their porosity mainly.

Therefore, for describing the angle dependencies and determining the filling factor, the so-called symmetrical Bruggeman effective medium approximation in the slightly modified form for spherical particles was used [30]:

Table 1
Summary of parameters for all studied structures (all abbreviations are defined in the text).

Structure	n	k	d_{eff}, nm	f_{Ge}, %
A	3.91	0.61	67.8	68.2 (50.0[a])
B	3.94	0.72	80.0	66.9
C	4.03	0.02	52.5	–
	4.60	0.26	8.0 (6.5[a])	47.5[a]

[a] From XRD measurements.

$$\sum_{i=1}^{N} f_i \frac{\tilde{\varepsilon}_i - \tilde{\varepsilon}_{eff}}{\tilde{\varepsilon}_i + (D-1)\tilde{\varepsilon}_{eff}} = 0, \quad (3)$$

where f_i and e_i are the filling fraction and dielectric permittivity of the i-th film component, $\tilde{\varepsilon}_{eff}$ is an effective film permittivity, D is the lattice dimensionality connected with depolarization factor ($D = 3$ is the most preferable value). Based on the experimental values of the optical constants of the films, the following values of the filling factors were obtained: $f_{Ge} = 68.2\%$ for structure A and $f_{Ge} = 66.9\%$ and $f_{Si} = 3.5\%$ for structure B. Filling the air voids near the surface of the Ge NCs by Si

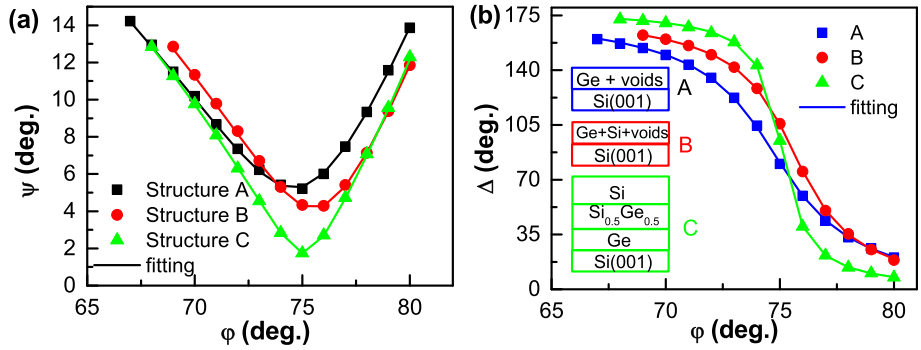

Fig. 4. Angle dependencies of the ellipsometric parameters of Ψ (a) and of Δ (b) for all structures - A, B and C.

adatoms decreased slightly the filling factor of the Ge.

Increasing the thickness of the Si capping layer results in a substantial change in optical constants of the structure C due to reconstruction of the surface of nc-Ge at Si deposition, Si-Ge interdiffusion and filling of the cavities with silicon. To determine the values of n and k for each layer from ellipsometric data, the three-layer model of the structure C was used: (i) capping layer of the intrinsic Si, (ii) interfacial layer $Si_{0.5}Ge_{0.5}$, and (iii) strained nanocrystalline layer with Ge in Si environment. The thickness of the interfacial layer was found to be 8.0 nm and coincided with the average value of the diameter of nc-Ge. The determined optical constants $n = 4.60$ and $k = 0.26$ proved to be consistent with tabulated values for $Si_{0.5}Ge_{0.5}$ solid solution. The following typical parameters have been obtained for the strained nanocrystalline layer with nc-Ge: $n = 4.03$, $k = 0.02$, $d_{eff} = 52.5$ nm. The resulting refractive index for this layer was lower than the tabulated value for bulk Ge. However, the absorption value was close to that of Si. The reason for this is that the space between the nanocrystallites is filled with Si.

Raman spectroscopy analysis was performed to answer the questions about the composition and values of elastic strain in the investigated Ge/Si heterostructures. Fig. 5a shows Raman spectra of all structures - A, B and C. The Ge-Ge phonon band with maxima at 302.4 cm^{-1} was observed for structure A. Additional deposition of Si with a nominal thickness of about 5 MLs shifts this peak to 303.3 cm^{-1} for structure B. Finally, Raman spectra of structure C with Ge NCs covered by 65-nm layer of Si reveals the bands at 298.3 cm^{-1} and 411.0 cm^{-1} corresponding to Ge-Ge vibrations and Si-Ge vibrations, correspondingly. For this structure, the Ge-Ge band may be presented as a sum of two Lorentz lines with maxima near 294.3 $cm^{-1}$and 302.3 cm^{-1} (see Fig. 5b).

Estimations of the composition and elastic strains of the nanocrystallites were made under the assumption that Ge nanocrystallites have a uniform composition and an immediate surrounding (shell of crystallites) in the structures coated with Si, is a strained $Si_{1-x}Ge_x$ solid solution.

The frequency positions of Si-Ge and Ge-Ge modes for a strained $Si_{1-x}Ge_x$ solid solution can be described as follows [31,32]:

$$\omega_{Si-Ge} = 400 + 29x - 95x^2 + 213x^3 - 170x^4 - b_s\varepsilon_{xx}, \quad (4)$$

$$\omega_{Ge-Ge} = 282.5 + 16x - b_s\varepsilon_{xx}, \quad (5)$$

where b_s is the phonon deformation potential with the composition dependence $b_s = b_4(x-1)^4 + b_0$, $b_4 = -190\ cm^{-1}$, b_0 equals to $-400\ cm^{-1}$ and $-575\ cm^{-1}$ for Ge-Ge and Si-Ge bands, respectively [33]. Using frequency positions of Ge-Ge and Si-Ge phonon bands and relations (1)–(3), the composition and values of the elastic strains for all investigated structures were determined (Table 2).

The average size of Ge nanocrystallites estimated from the full-width of the Ge phonon peak in correlation length model of phonon confinement [34] is 5–6 nm for the structure A and 6–7 nm for the structure B. The corresponding low-frequency shift of the Ge phonon band due to phonon confinement effect for the structure A (B) is expected to be about 3.5 (2.8) cm^{-1}. However, in our case the 1.9 (2.8) cm^{-1} blue shift relatively to Ge-bulk phonon frequency (300.5 cm^{-1}) is observed. Thus, the total up-shift amounts to 5.4 (5.6) cm^{-1}, which testifies the compressive stress in the Ge nanocrystals acting in the opposite direction to the phonon confinement effect were obtained. Thus, the estimated compressive strain is $\varepsilon_{xx} \sim -0.0124$ and -0.0129 for the structures A and B, respectively [35].

Therefore all our studies, i.e. atomic force microcopy, X-ray measurements, multi-angle ellipsometry as well as Raman spectroscopy have shown that thin Ge films formed on Si(001) substrate by low temperature epitaxy of Ge on Si(001) at 350 °C and s growth rate, about 5 nm/min, had a crystalline structure and consisted of Ge NCs of 5–6 nm in size, which were pseudomorphic to the substrate. The size of NCs was much smaller than the Ge film thickness, estimated by the ellipsometry method and then the average diameter of the surface nanostructures determined from the analysis of AFM images (see Fig. 1). This means that the films consist of several layers of crystalline NCs, the space between them is filled with air and contains amorphous phase of Ge. An air volume fraction in the structure A, $1 - f_{Ge} = 31.8\%$, was determined by the method of Bruggeman effective medium approximation. The effective coefficient of absorption of the film ($k = 0.61$) was close to the tabulated values for crystalline Ge. Since the absorption coefficient of amorphous Ge at $\lambda = 632.8$ nm is significantly less than the experimental value and is $k = 0.05$, a conclusion may be drawn that the films are characterized by a high degree of crystallinity.

Deposition of Si adatoms on the film surface stimulates the reconstruction of the surface with Ge NCs and increases the degree of Ge crystallinity. The similar surface reconstruction was described previously for Ge NCs grown on oxidized surface of Si(001) [36]. This is confirmed by changes in Raman spectra and in reciprocal space maps. In addition, AFM images revealed a coalescence of adjacent NCs, mostly of small sizes.

Let us analyze in more detail the change in optical properties and morphology of the films at silicon deposition on the Ge NCs surface. The structure B showed the increased intensity of the Ge-Ge peak with the decreased full-width as compared with the initial structure A. This is due to crystallization of the Ge thin films facilitated by silicon deposition. It can be suggested that at the initial stages of epitaxy the Si adatoms are selectively linked only to dangling Ge bonds at the surface of the NCs. Due to the lattice mismatch between Ge and Si, the elastic

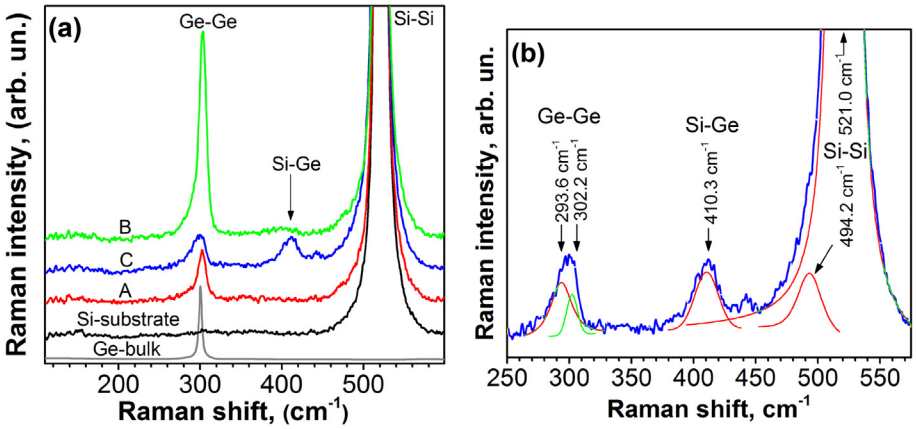

Fig. 5. (a) Raman spectra of structures A, B, and C. Raman spectrum of the Si substrate is given for comparison. The layout of the experiment: $z(x,y)\bar{z}$, $\lambda_{exc} = 488$ nm, T = 300 K. Raman spectra of Si substrate and bulk Ge are given for reference (b) Raman spectrum of structure C with Ge-Ge vibration peak decomposed into two Lorentz lines with maxima near 293.6 cm^{-1} and 302.2 cm^{-1}.

Table 2
Experimental phonon frequencies (ω) and the full-widths (Γ) of the phonon modes, compositions (x) of $Si_{1-x}Ge_x$ solid solution and elastic strains (ε_{xx}) of NCs.

Structure	Ge-Ge		Si-Ge		Si-Si		x_{Ge}	ε_{xx}
	ω, cm^{-1}	Γ, cm^{-1}	ω, cm^{-1}	Γ, cm^{-1}	ω, cm^{-1}	Γ, cm^{-1}		
A	302.4	11.5	–	–	–	–	1	−0.0124
B	303.3	10.3	397.2	48.5	477.2	20.1	–	−0.0129
C	293.6	20.4	410.3	23.1	494.2	22.5	0.48	−0.0073
	302.2	10.1	–	–	–	–		−0.0085

energy accumulated during Si deposition. At the same time, the distance between the neighboring Ge nanocrystallites reduced. While reaching the critical magnitude of deformation, the total energy of the system can decrease at the expense of a collapse of spacing between neighboring NCs and due to the reduction of the surface energy. Coalescence of NCs occurs when the sum of the elastic energy, generated at the unit area, and of the grain boundary energy is equal to the energy of two free surfaces of the separate nanocrystallites. Their aggregation into NCs facilitated by the epitaxy of the linking material – Si. At the same time, the amorphous Ge phase will be further used and the degree of the film crystallinity will rise. The evidence of the described crystallization is the polygonal base of the formed SiGe NCs (see Fig. 1b) and substantial (by a factor of 3) increase of the Ge-Ge peak area in Raman spectra of the structure B after Si deposition. The process of crystallization accompanied also by slight Si-Ge mixing, which led to the formation of $Si_{0.08}Ge_{0.92}$ alloy and to the appearance of Si-Ge vibration mode near 397.2 cm^{-1}. The ratio of peak intensities of Si-Ge and Ge-Ge vibrations for the structure B indicates that contributions both of Ge nanocrystallites and of their $Si_{0.08}Ge_{0.92}$ interfacial layers are present in the Raman spectrum. Note that Si atoms "unused" during coalescence and formation of the solid solution, fill the cavities between NCs.

In the case of the structure C, the epitaxy of the Si capping layer on the Ge nanocrystalline surface led to a more significant Si-Ge mixing and to the formation of the solid solution with the lower Ge content that is $Si_{0.5}Ge_{0.5}$. The Ge-Ge peak of this structure contains contributions of two phases: Ge nanocrystallites near 302.3 cm^{-1} and $Si_{0.5}Ge_{0.5}$ solid solution at about 294.3 cm^{-1} (see Fig. 5b). The formation of the solid solution occurred in the process of filling the cavities between Ge NCs by silicon atoms. However, the core of NCs remained to consist of pure Ge, while their interfaces proved to consist of the solid solution. Optical constants of this effective medium had significantly changed and approached the values typical for silicon films with Ge inclusions. The effective thickness of $Si_{0.5}Ge_{0.5}$ layer, that is $d = 6.5$ nm, was determined on the basis of X-ray reflectivity measurements. This thickness is consistent with the size of Ge nanocrystallites in the structures A and B. This means that the most significant Si-Ge mixing occurred only in the upper layer of nanocrystallites, while the content of the underlying Ge crystallites remained unchanged.

4. Conclusions

By using the methods of Raman scattering, multi-angle ellipsometry and X-ray measurements, the changes of optical properties and morphology of thin films with Ge NCs are studied as a result of Si adatoms deposition on the film surface. It is shown that low-temperature Ge epitaxy on Si(001) surface at 350 °C and at high (about 5 nm/min) growth rate leads to the formation of nanocrystalline films consisting of Ge crystallites, of 5–6 nm in size, which are pseudomorphic to the substrate. The porosity of the films is about 50%.

Deposition of Si adatoms on the film surface stimulates the reconstruction of the surface with nanocrystallites and results in the increase of the degree of Ge crystallinity and in a slight Si-Ge mixing. This was confirmed by the changes in the shapes of Raman spectra as well as of the reciprocal space maps. AFM images revealed the coalescence of adjacent NCs, mostly of small in size. The changes in the values of the optical constants determined by analyzing the data obtained by the multi-angle ellipsometry method are described by means of Bruggeman approximation. The main reasons for these changes are the film crystallization and the presence of Si crystalline phase in the structures with Si capping layer. The prepared Ge nanocrystalline films, as well as the films covered with Si, may be used in quantum dot solar cells due to the high absorption capacity of the films.

References

[1] Z.C. Holman, Chin-Yi Liu, U.R. Kortshagen, Germanium and silicon nanocrystal thin-film field-effect transistors from solution, Nano Lett. 10 (2010) 2661.
[2] K. Brunner, Si/Ge nanostructures, Rep. Prog. Phys. 65 (2002) 27.
[3] J. Liu, M. Beals, A. Pomerene, S. Bernardis, R. Sun, J. Cheng, L.C. Kimerling, J. Michel, Waveguide-integrated, ultralow-energy GeSi electro-absorption modulators, Nat. Photonics 2 (2008) 433–437.
[4] S. Cosentino, P. Liu, S.T. Le, S. Lee, D. Paine, A. Zaslavsky, D. Pacifici, S. Mirabella, M. Miritello, I. Crupi, A. Terrasi, High-efficiency silicon-compatible photodetectors based on Ge quantum dots, Appl. Phys. Lett. 98 (2011) 221107.
[5] Y.M. Niquet, G. Allan, C. Delerue, M. Lannoo, Quantum confinement in germanium nanocrystals, Appl. Phys. Lett. 77 (2000) 1182.
[6] C. Bulutay, Interband, intraband, and excited-state direct photon absorption of silicon and germanium nanocrystals embedded in a wide band-gap lattice, Phys. Rev. B 76 (2007) 205321.
[7] S. Das, R.K. Singha, A. Dhar, S.K. Ray, A. Anopchenko, N. Daldosso, L. Pavesi, Electroluminescence and charge storage characteristics of quantum confined germanium nanocrystals, J. Appl. Phys. 110 (2011) 024310.
[8] J. Ni, Q. Liu, J.J. Zhang, J. Ma, H. Wang, X.D. Zhang, Y. Zhao, Microcrystalline silicon-germanium solar cells with spectral sensitivities extending into 1300 nm, Sol. Energy Mater. Sol. Cells 126 (2014) 6–10.
[9] Chang Li, Jian Ni, Xiaoxiang Sun, Xinyu Wang, Zhenglong Li, Hongkun Cai, Juan Li, Jianjun Zhang, Nanocrystalline germanium nip solar cells with spectral sensitivities extending into 1450 nm, J. Phys. D. Appl. Phys. 50 (2017) 045108.
[10] D. Carolan, Recent advances in germanium nanocrystals: synthesis, optical properties and applications, Prog. Mater. Sci. 90 (2017) 128.
[11] V.S. Lysenko, Y.V. Gomeniuk, V.N. Kudina, N.P. Garbar, S.V. Kondratenko, Ye Melnichuk, Y.N. Kozyrev, Hopping conduction and LF noise in structures with Ge nanoclusters grown on oxidized Si(001), J. Mater. Sci. 51 (2016) 8799.
[12] V.A. Egorov, G.É. Cirlin, A.A. Tonkikh, V.G. Talalaev, A.G. Makarov, N.N. Ledentsov, V.M. Ustinov, N.D. Zakharov, P. Werner, Si/Ge nanostructures for optoelectronics applications, Phys. Solid State 46 (2004) 49–55.
[13] V.S. Lysenko, Yu.V. Gomeniuk, V.V. Strelchuk, A.S. Nikolenko, S.V. Kondratenko, Yu.N. Kozyrev, M.Yu. Rubezhanska, C. Teichert, Carrier transfer effect on transport in p-i-n structures with Ge quantum dots, Phys. Rev. B 84 (2011) 115425.
[14] D.J. Eaglesham, M. Cerullo, Dislocation-free Stranski–Krastanov growth of Ge on Si (100) Phys, Rev. Let. 64 (1990) 1943.
[15] C. Teichert, Self-organization of nanostructures in semiconductor heteroepitaxy, Phys. Rep. 365 (2002) 335.
[16] A. Pimpinelli, J. Villain, Physics of Crystal Growth, Cambridge University Press, Cambridge, UK, 1998.
[17] J. Zhang, M. Brehm, M. Grydlik, O.G. Schmidt, Evolution of epitaxial semiconductor nanodots and nanowires from supersaturated wetting layers, Chem. Soc. Rev. 44 (2015) 26.
[18] J. Michel, J. Liu, L.C. Kimerling, High-performance Ge-on-Si photodetectors, Nat. Photonics 4 (2010) 527–534.
[19] D. Nam, D. Sukhdeo, A. Roy, K. Balram, S.-L. Cheng, K.C.-Y. Huang, Z. Yuan, M. Brongersma, Y. Nishi, D. Miller, K. Saraswat, Strained germanium thin film membrane on silicon substrate for optoelectronics, Opt. Express 19 (2011) 25866–25872.
[20] S.V. Kondratenko, O.V. Vakulenko, Y.N. Kozyrev, M.Y. Rubezhanska, A.G. Naumovets, A.S. Nikolenko, C. Teichert, Photovoltaic properties and photoconductivity in multilayer Ge/Si heterostructures with Ge nanoislands, J. Mater. Sci. 46 (2011) 5737–5742.
[21] A. Rastelli, M. Stoffel, G. Katsaros, J. Tersoff, U. Denker, T. Merdzhanova, O.G. Schmidt, Reading the footprints of strained islands, Microelectron. J. 37 (2006) 1471.
[22] M. Brehm, H. Lichtenberger, T. Fromherz, G. Springholz, Ultra-steep side facets in

multi-faceted SiGe/Si(001) Stranski–Krastanow islands, Nanoscale Res. Lett. 6 (2011) 70.
[23] C.S. Peng, Q. Huang, W.Q. Cheng, J.M. Zhou, Y.H. Zhang, T.T. Sheng, C.H. Tung, Optical properties of Ge self-organized quantum dots in Si, Phys. Rev. B 57 (1998) 8805.
[24] A.A. Shklyaev, M. Shibata, M. Ichikawa, High-density ultrasmall epitaxial Ge islands on Si(111) surfaces with a SiO_2 coverage, Phys. Rev. B 62 (2000) 1540.
[25] B.I. Shklovskii, B.Z. Spivak, Scattering and interference effects in variable range hopping, Hop. Trans. Sol. 28 (1991) 271.
[26] M. Chaldek, V. Valvoda, C. Dorner, C. Holy, J. Grim, Quantitative study of interface roughness replication in multilayers using X-ray reflectivity and transmission electron microscopy, Appl. Phys. Lett. 69 (1996) 1318.
[27] V.P. Kladko, A.V. Kuchuk, P.M. Lytvyn, O.M. Yefanov, N.V. Safriuk, A.E. Belyaev, Yu.I. Mazur, E.A. DeCuir Jr., M.E. Ware, G.J. Salamo, Substrate effects on the strain relaxation in GaN/AlN short-period superlattices, Nanoscale Res. Lett. 7 (2012) 289.
[28] V.O. Yukhymchuk, A.M. Yaremko, M.Y. Valakh, A.V. Novikov, E.V. Mozdor, P.M. Lytvyn, Z.F. Krasilnik, V.P. Kladko, V.M. Dzhagan, N. Mestres, J. Pascual, Theoretical and experimental investigations of single- and multilayer structures with Si Ge nanoislands, Mater. Sci. Eng. 23 (2003) 1027–1031.
[29] D.E. Aspnes, A.A. Studna, Dielectric functions and optical parameters of Si, Ge, GaP, GaAs, GaSb, InP, InAs, and InSb from 1.5 to 6.0 ev, Phys. Rev. B 27 (1983) 985.
[30] D.A.G. Bruggeman, Berechnung verschiedener physikalischer Konstanten von heterogenen Substanzen I. Dielektrizitätskonstanten und Leitfähigkeiten der Mischkörper aus isotropen Substanzen, Ann. Phys. 24 (1935) 636.
[31] S.F. Ren, W. Cheng, P.Y. Yu, Microscopic investigation of phonon modes in SiGe alloy nanocrystals, Phys. Rev. B 69 (2004) 235327.
[32] M.I. Alonso, M. de la Calle, J.O. Osso, Strain and composition profiles of self-assembled Ge/Si (001) islands, J. Appl. Phys. 98 (2005) 033530.
[33] J.S. Reparaz, A. Bernardi, A.R. Goni, Composition dependence of the phonon strain shift coefficients of SiGe alloys revisited, Appl. Phys. Lett. 92 (2008) 081909.
[34] A. Wellner, V. Paillard, C. Bonafos, H. Coffin, A. Claverie, B. Schmidt, K.H. Heinig, Stress measurements of germanium nanocrystals embedded in silicon oxide, Appl. Phys. 94 (2003) 5639.
[35] A. Gassenq, S. Tardif, K. Guilloy, I. Duchemin, N. Pauc, D. Rouchon, J.M. Hartmann, J. Widiez, Y.M. Niquet, R. Geiger, T. Zabel, H. Sigg, J. Faist, A. Chelnokov, F. Rieutord, V. Reboud, V. Calvo, Raman-strain relations in highly strained Ge: uniaxial ⟨100⟩, ⟨110⟩ and biaxial (001) stress, J. Appl. Phys. 121 (2017) 055702.
[36] V.S. Lysenko, S.V. Kondratenko, Y.N. Kozyrev, V.P. Kladko, Y.V. Gomeniuk, Y.Y. Melnichuk, N.B. Blanchard, Surface reconstruction and optical absorption changes for Ge nanocrystallites grown on chemically oxidized Si(100) surfaces, Sci. Semicond. Tech. 28 (2013) 1–9 085009.